THE JOURNAL OF PHYSICAL CHEMISTRY B

Article

Electrogenerated Chemiluminescence. 65. An Investigation of the Oxidation of Oxalate by Tris(polypyridine) Ruthenium Complexes and the Effect of the Electrochemical Steps on the Emission Intensity

Frdric Kanoufi, and Allen J. Bard

J. Phys. Chem. B, **1999**, 103 (47), 10469-10480 • DOI: 10.1021/jp992368s

Electrogenerated Chemiluminescence. 65. An Investigation of the Oxidation of Oxalate by Tris(polypyridine) Ruthenium Complexes and the Effect of the Electrochemical Steps on the Emission Intensity

Frédéric Kanoufi and Allen J. Bard*

Department of Chemistry and Biochemistry, The University of Texas at Austin, Austin, Texas 78712

Received: July 14, 1999; In Final Form: September 15, 1999

The homogeneous oxidation of oxalate has been investigated at an ultramicroelectrode by means of redox catalysis with different iron and ruthenium coordination complexes. Kinetically, the process is governed by the first electron transfer. It can be rationalized by Marcus theory. When the electron acceptor is a ruthenium coordination complex, the second electron transfer can generate a luminescent excited state of the ruthenium. This electrochemiluminescent process is related, in a first approximation, to the catalytic efficiency of the homogeneous oxalate oxidation, but also to the different competing routes for the second electron transfer (oxidation of $CO_2^{\bullet -}$). The effect of the pH and the ionic strength on the redox catalysis and the light emission are discussed.

Introduction

Electrogenerated chemiluminescence (ECL) involves the formation of electronically excited states by an energetic electron transfer (ET) between redox species generated at an electrode surface. The earliest ECL reactions[1] were carried out in aprotic solvents and occurred by the annihilation reaction of two oppositely charged radical ions, $R^{\bullet +}$ and $R^{\bullet -}$.

ECL reactions can be observed in aqueous solution, even with the rather small potential window available in water, based on the ability to generate energetic reactants upon bond cleavage of a coreactant. For example, light emission is found during the electrochemical oxidation of tris(2,2′-bpyridine)ruthenium-(II) ($Ru(bpy)_3^{2+}$) and oxalate ($C_2O_4^{2-}$). The mechanism proposed for this ECL is[2]

$$Ru(bpy)_3^{2+} - e \rightarrow Ru(bpy)_3^{3+}$$

$$C_2O_4^{2-} - e \rightarrow C_2O_4^{\bullet -}$$

$$Ru(bpy)_3^{3+} + C_2O_4^{2-} \rightarrow Ru(bpy)_3^{2+} + C_2O_4^{\bullet -}$$

$$C_2O_4^{\bullet -} \rightarrow CO_2 + CO_2^{\bullet -}$$

$$Ru(bpy)_3^{3+} + CO_2^{\bullet -} \rightarrow Ru(bpy)_3^{2+}* + CO_2$$

There is strong interest in such ECL reactions because $Ru(bpy)_3^{2+}$ can be used as a label in immunoassays and DNA probes and because these systems, with species such as oxalate and tri-*n*-propylamine, depend on coreactant chemistry. Although these systems have been of practical importance, details of the kinetics and mechanisms of the reactions involved have been sparse. Optimization of these systems clearly depends on a better understanding of the reactions and how they affect the efficiency of light emission.

We have thus undertaken an electrochemical study of the reaction of oxalate with several Ru and Fe compounds containing bpy-related ligands. An important mechanistic aspect of the study was to find out if the ET and the bond-breaking step in the oxalate oxidation occur successively or simultaneously, i.e., whether the radical anion, $C_2O_4^{\bullet -}$, is a true intermediate. In the former case, the ET is of the outer-sphere type and can be described by the Marcus model.[3] When the bond breaking and ET are concerted, the ET has an inner-sphere character and can be described by the dissociative ET model developed by Savéant.[4]

Although this latter route conflicts with the observed lifetime in the microsecond region for the oxalate radical anion $C_2O_4^{\bullet -}$,[5] an inner-sphere mechanism has been proposed when the ET is mediated homogeneously during luminescence quenching of the excited states of chromium(III) polypyridyl complexes (CrL_3^{3+}*) by oxalate,[6] or in possible oxalate oxidation by the stable tris-(acetylacetonato)−manganese(III) complex.[7] On the other hand, in homogeneous ET to oxalate photoinduced by the methyl viologen dication,[5a] the tris(bpyrazine)ruthenium(II)[8] excited state, or the tris(sepulchrate)−cobalt(III),[9] the $C_2O_4^{\bullet -}$ fragmentation, if it occurs, is proposed to be faster than the escape from the solvent cage, suggesting specific interactions in the solvent cage between the oppositely charged species. In these experiments, an inner-sphere ET is not precluded.

In the work reported here, we characterize in more detail the homogeneous oxalate oxidation mediated by different electrochemically generated ruthenium(III) or iron(III) complexes containing bpy-type ligands. The ECL arising from the ET with the ruthenium species is then discussed and related to the oxalate oxidation kinetics. The homogeneous oxalate oxidation is then interpreted in terms of the different ET models. An attempt is then made to discuss the dependence of the ECL process in terms of standard potentials of the different Ru complexes. In these studies we make use of ultramicroelectrodes because past studies with the scanning electrochemical microscope (SECM)[10] probed the homogeneous ET and ECL emission and demonstrated that they provide steady-state currents and light intensities. The ability to use steady-state methods, as shown below, simplifies the theoretical treatment compared to the transient methods employed earlier.[2b]

Experimental Section

Chemicals. Oxalic acid and $Na_2C_2O_4$ from J. T. Baker (Phillipsburg, NJ), $Ru(bpy)_3Cl_2$ hexahydrate from Strem Chemi-

10.1021/jp992368s CCC: $18.00
Published on Web 11/04/1999

SCHEME 1

$$P - e \rightleftharpoons Q$$

$$Q + C_2O_4^{2-} \underset{k_{-0}}{\overset{k_0}{\rightleftharpoons}} P + C_2O_4^{\bullet -} \quad (0)$$

$$C_2O_4^{\bullet -} \xrightarrow{k_1} CO_2 + CO_2^{\bullet -} \quad (1)$$

or $$Q + C_2O_4^{2-} \xrightarrow{k_0} P + CO_2^{\bullet -} + CO_2 \quad (0')$$

then $$Q + CO_2^{\bullet -} \xrightarrow{k_2} P + CO_2 \quad (2)$$

cals (Newburyport, MA), tris(9,10-phenanthroline)ruthenium-(II) ($Ru(phen)_3^{2+}$) chloride anhydrous from Johnson Matthey (Ward Hill, MA) and all the salts were used as-received. The different tris(polypyridine)ruthenium(II) and -iron(II) complexes were synthesized according to reported procedures.[11] The aqueous solutions were prepared from deionized water (Milli-Q, Millipore).

Electrode and Electrochemical Cells. Carbon fibers of 3.5-μm radius and Pt wires of 12.5- and 25-μm radius (Goodfellow, Cambridge, U.K.) were heat-sealed in glass capillaries under vacuum and then polished to produce ultramicroelectrodes as previously described.[12] They were polished with 0.05-μm alumina and rinsed with deionized water before each experiment. A three-electrode configuration was employed in all experiments with a 0.2-mm diameter Pt wire as the counter electrode and Ag/AgCl as the reference electrode. However, all potentials are reported vs the NHE. All the experiments were carried out in solutions deaerated by nitrogen bubbling.

Apparatus and Procedure. Cyclic voltammetric experiments were performed utilizing a Bioanalytical Systems (West Lafayette, IN) model-100A electrochemical analyzer. Cyclic voltammograms with simultaneous photon detection were recorded using a home-built potentiostat in conjunction with a photomultiplier tube (PMT, Hamamatsu R4220p or R928) installed under the electrochemical cell and connected to an operational amplifier-based current-to-voltage converter and voltage amplifier.[10]

Results and Discussion

Redox Catalysis of the Oxalate Oxidation. The principle of the method[13] is summarized in Scheme 1. P/Q represents a reversible couple that can mediate the homogeneous ET to the oxalate species. Two possible paths can be assumed for the first ET reaction between Q and oxalate, depending on the intermediacy of the oxalate radical anion. Reactions 0 and 1 assume the formation of the intermediate oxalate anion radical $C_2O_4^{\bullet -}$, while reaction 0′,which leads directly to carbon dioxide and $CO_2^{\bullet -}$, accounts for a dissociative ET path. Because $CO_2^{\bullet -}$ is a strong reductant ($E° = -1.9$ V vs NHE[14]), it is more easily oxidized by Q than the starting oxalate moiety. Its oxidation by reaction 2 leads to a second carbon dioxide molecule.

The redox catalysis experiments were carried out at ultramicroelectrodes of different sizes and material (carbon radius, 3.5 μm; platinum radii, 12 and 25 μm).

Determination of Rate Constant Using Ultramicroelectrodes. The experiment involves measuring the steady-state plateau current of the mediator oxidation in the absence (i_{s0}) and in the presence (i_s) of oxalate (Figure 1). In the absence of oxalate, the steady-state current at an ultramicroelectrode is given by

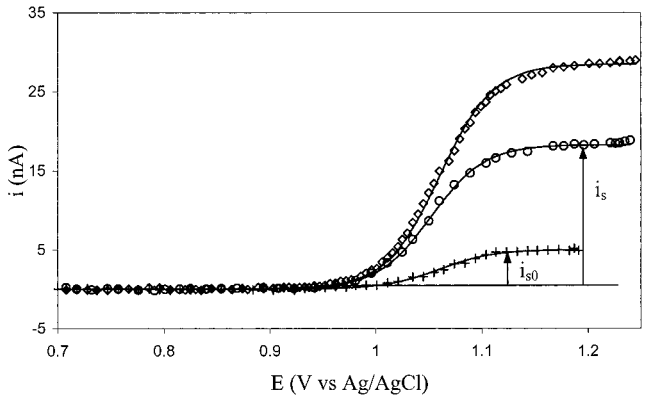

Figure 1. Voltammograms of 1 mM $Ru(bpy)_3^{2+}$ in 0.1 M NaCl + 0.1 M phosphate buffer, pH 6.1, at a 50-μm diameter Pt electrode, scan rate $v = 10$ mV/s (+) in absence and in the presence of (○) 1 mM and (◇) 2 mM oxalate, $C_2O_4^{2-}$. (+,○,◇) Experimental and (—) simulated voltammograms according to eq 10; see text.

$$i_{s0} = 4naFD[P]^0 \quad (3)$$

where a is the electrode radius, D and $[P]^0$ are, respectively, the diffusion coefficient and the initial concentration of P, n is the number of electrons involved, and F is the Faraday constant.

Kinetic and mechanistic information can be derived from the variation of the catalytic efficiency, defined as the ratio of the plateau currents i_s/i_{s0}, with the oxalate and mediator concentration. The theoretical expression leading to the variation of the catalytic efficiency with the oxalate concentration has been established for the EC′ mechanism (reaction 0 or 0′).[15] Because all our experiments were made in the presence of excess oxalate, its concentration can be considered as constant and the catalytic efficiency is given by[15b,c]

$$\frac{i_s}{i_{s0}} = 1 + \frac{\pi a}{4}\left(\frac{k_0[Ox]^0}{D}\right)^{1/2} \quad (4)$$

where a is the radius of the ultramicroelectrode, D is the P/Q diffusion coefficient, $[Ox]^0$ is the oxalate concentration, and k_0 is the homogeneous ET (reaction 0 or 0′) rate constant. We assume throughout this treatment that the diffusion coefficients for all of the species are equal. For a dissociative ET, because the carbon dioxide anion radical, $CO_2^{\bullet -}$, is more easily oxidized by Q than the starting compound, we can consider its concentration to be at steady state so that

$$\partial[CO_2^{\bullet -}]/\partial t = 0 = k_0[Ox][Q] - k_2[CO_2^{\bullet -}][Q] \quad (5)$$

The solution of the diffusion equation should thus result in the replacement of $[Ox]^0$ by $2[Ox]^0$ (i.e., every oxalate oxidized will result in the overall passage of two electrons), so the previous expression of the catalytic efficiency (eq 4) leads to

$$\frac{i_s}{i_{s0}} = 1 + \frac{\pi a}{4}\left(\frac{2k_0[Ox]^0}{D}\right)^{1/2} \quad (6)$$

The theoretical solution of the diffusion equation, when taking into account the complete Scheme 1 (reactions 0, 1, and 2), has been proposed in the case of stationary and quasi-stationary methods at large electrodes,[16] but not, to our knowledge, at ultramicroelectrodes. At ultramicroelectrodes, one can treat the

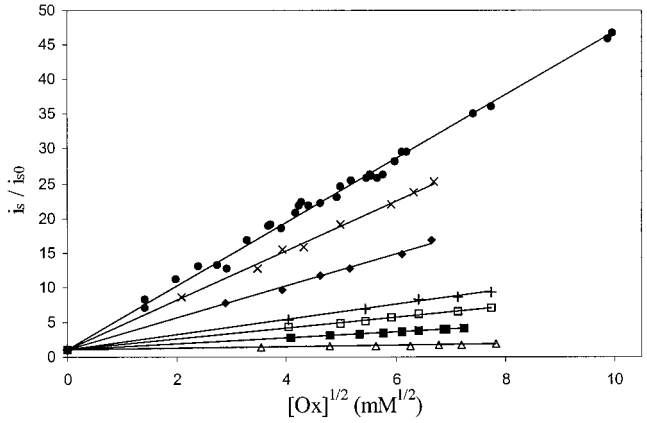

Figure 2. Variation of the catalytic efficiency, i_s/i_{s0}, with the square root of the oxalate concentration $[Ox]^{1/2}$ for different redox catalysts in 0.1 M NaCl + 0.1 M phosphate buffer, pH 6.1. From top to bottom (●) 0.1 < $[Ru(bpy)_3^{2+}]$ < 4.4 mM; (×) 0.25 < $[Ru(phen)_3^{2+}]$ < 0.8 mM; (◆) 0.5 < $[Ru(dmbp)(bpy)_2^{2+}]$ < 0.9 mM; (+) 0.15 < $[Ru(dmphen)_3^{2+}]$ < 0.25 mM; (□) 0.15 < $[Ru(dmbp)_3^{2+}]$ < 0.3 mM; (■) 0.65 < $[Fe(bpy)_3^{2+}]$ < 1 mM; (△) 0.14 < $[Fe(dmbp)_3^{2+}]$ < 0.24 mM.

system at steady state, and under the conditions discussed below, steady-state approximations can be made for the different reaction intermediates. Reaction 1, if it occurs, is known to be relatively fast. A value of $k_1 \approx 2 \times 10^6$ s^{-1} was obtained by pulse radiolysis in aqueous solution,[5] but the same authors proposed a much higher value (a lifetime shorter than 1 ns) when the oxidation involves a homogeneous electron acceptor. In any case, it is reasonable to consider the oxalate and carbon dioxide radicals anions concentrations to be at steady state. Under these conditions, the following expressions hold:

$$\partial[C_2O_4^{\bullet -}]/\partial t = 0 = k_0'[Ox][Q] - k_{-0}[C_2O_4^{\bullet -}][P] - k_1[C_2O_4^{\bullet -}] \quad (7)$$

$$\partial[CO_2^{\bullet -}]/\partial t = 0 = k_1[C_2O_4^{\bullet -}] - k_2[CO_2^{\bullet -}][Q] \quad (8)$$

The diffusion equation for Q then becomes

$$\frac{\partial[Q]}{\partial t} = D\frac{\partial^2[Q]}{\partial r^2} - \frac{D}{r}\frac{\partial[Q]}{\partial r} - \frac{2k_0[C_2O_4^{2-}]^0[Q]}{k_1 + k_{-0}[P]} \quad (9)$$

As previously reported in the general solution of the problem,[16,17] two limiting situations are expected according to the competition between the backward ET ($k_{-0}[P]^0$) and the bond dissociation step (k_1). When $k_1 \gg k_{-0}[P]^0$, the homogeneous ET kinetically governs the reaction and the variation of the catalytic efficiency is given by eq 6. If $k_1 \ll k_{-0}[P]^0$, the rate-determining step is the chemical reaction, with the homogeneous ET acting as a pre-equilibrium. The diffusion equation has not been solved in this case, but the catalytic efficiency should depend on both the oxalate and mediator concentration.[18]

Because in all of our experiments (Figure 2) the catalytic efficiency depended solely on the oxalate concentration but not on the mediator concentration, it seems clear that the reaction is always kinetically controlled by the homogeneous ET. For this reason, we did not attempt to solve the diffusion equation for the case of kinetic control by the following chemical step.

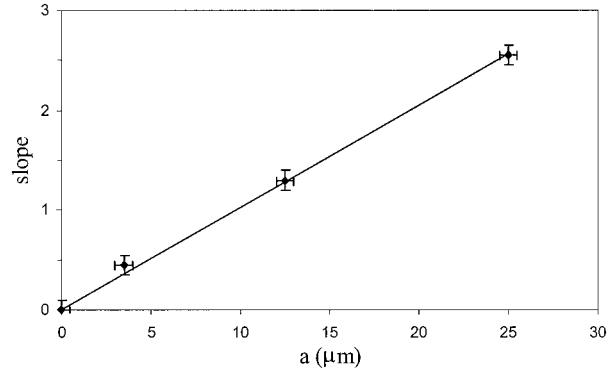

Figure 3. Variation of the slope extracted from Figure 2 with the ultramicroelectrode radius for the homogeneous oxidation of oxalate by $Ru(bpy)_3^{2+}$ in 0.1 M NaCl + 0.1 M phosphate buffer, pH 3. Pt ultramicroelectrodes radii, 12.5 and 25 μm; carbon fiber ultramicroelectrode radius, 3.5 μm.

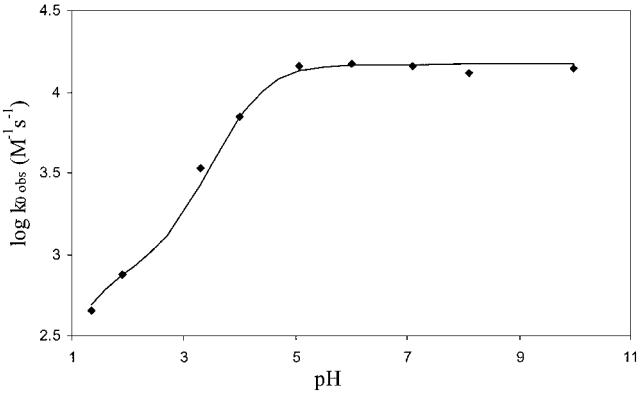

Figure 4. Variation of the logarithm of the observed homogeneous rate constant, log k_{0obs}, with the pH for the $Ru(bpy)_3^{2+}$/oxalate system in 0.1 M NaCl + 0.1 M phosphate buffer, except for pH 1.4 (0.2 M H_3PO_4). (◆) Experimental values and (—) simulated variations according to eq 11; see text.

An expression of the voltammogram can then be given by the general equation of the voltammetric wave[19]

$$i(E) = \frac{i_s}{1 + \exp\left(-\frac{F}{RT}(E - E_{1/2})\right)} \quad (10)$$

where E is the electrode potential and $E_{1/2}$ the half wave potential of the oxidation. As shown in Figure 1, there is good agreement between this expression and the experimental voltammograms.

Generally, the rate constants for the homogeneous ET between the redox mediator and oxalate were obtained from the slope (equal to $(\pi a/4)(2k_0/D)^{1/2}$) of the variation of the catalytic efficiency i_s/i_{s0}, with the square root of the oxalate concentration. Figure 2 summarizes the results for different mediators. For each mediator, the experimental points fall along a single line. As expected from eq 6, the value of the slope increases linearly with the ultramicroelectrode radius (Figure 3). To enhance the catalytic effect and therefore the electrochemical response of the system, a 50-μm diameter Pt electrode was preferred for the kinetic studies.

pH Dependence of the Rate Constant. The homogeneous rate constants for ET between $Ru(bpy)_3^{2+}$ and the oxalate anion obtained from eq 6 at different pHs are given in Figure 4. For pH > 5, k_{0obs} is almost independent of the pH, but it

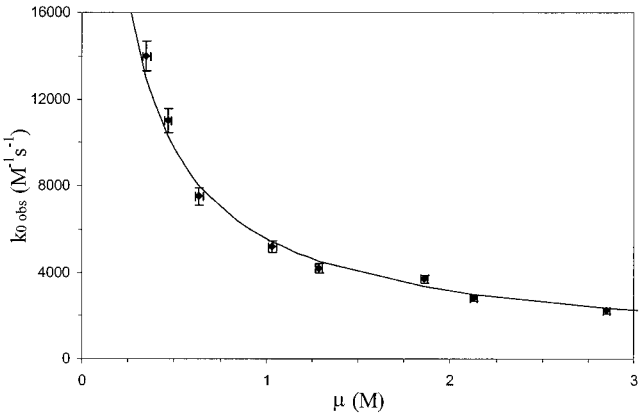

Figure 5. Variation of the observed homogeneous rate constant, k_{0obs}, with the ionic strength, μ, for the $Ru(bpy)_3^{2+}$/oxalate system in unbuffered Na_2SO_4 solutions. (■) Experimental values and (—) theoretical variation according to eq 15.

SCHEME 2

$$Ru(bpy)_3^{3+} + C_2O_4^{2-} \xrightarrow{k_0} Ru(bpy)_3^{2+} + \text{product} \quad (0)$$

$$Ru(bpy)_3^{3+} + HC_2O_4^{-} \xrightarrow{k_{0h}} Ru(bpy)_3^{2+} + \text{product} \quad (0h)$$

$$Ru(bpy)_3^{3+} + H_2C_2O_4 \xrightarrow{k_{0hh}} Ru(bpy)_3^{2+} + \text{product} \quad (0hh)$$

decreases dramatically for pH < 5. This effect is attributed to the acid−base behavior of oxalic acid ($pK_{a1} = 1.23$; $pK_{a2} = 4.19$).[20]

To explain this behavior, the ET between $Ru(bpy)_3^{2+}$ and the different oxalate species ($C_2O_4^{2-}$; $HC_2O_4^{-}$; $H_2C_2O_4$), as depicted in Scheme 2, was considered. Whatever product is formed during the first ET, these steps are rate-determining for the global oxidation process.

According to this scheme, the variation of the apparent rate constant with the pH is given by

$$k_{0obs} = \frac{k_0 + k_{0h}\frac{[H^+]}{K_{2a}} + k_{0hh}\frac{[H^+]^2}{K_{2a}K_{1a}}}{1 + \frac{[H^+]}{K_{2a}} + \frac{[H^+]^2}{K_{2a}K_{1a}}} \quad (11)$$

The best fit (Figure 4) of our experimental data by eq 11 is obtained when using the following values: $k_0 = 1.4 \times 10^4\ M^{-1}\ s^{-1}$, $k_{0h} = 8 \times 10^2\ M^{-1}\ s^{-1}$, $k_{0hh} \approx 0$, $pK_{a1} = 1.2$, and $pK_{a2} = 4.1$. The pK_a values found in this fit are in good agreement with the tabulated ones.[20] The difference between the ET rate constants, k_0 and k_{0h}, are also fit with the intuitive feeling that $HC_2O_4^-$ should be more difficult to oxidize than $C_2O_4^{2-}$.

Effect of Ionic Strength on the Homogeneous Rate Constant. The ionic strength affects the homogeneous ET rate constant between $Ru(bpy)_3^{2+}$ and $C_2O_4^{2-}$, as shown in Figure 5. The ionic strength influence was studied in unbuffered Na_2SO_4 solutions, where an increase in the ionic strength tended to decrease the rate previously with both tris(polypyridine)-ruthenium complexes[21] and oxalate.[6] This decrease has been attributed to the existence of an ion-pairing equilibrium preceding the ET. Ion pair formation occurs with most carboxylates and especially oxalate.[22] For example, ion-pair formation with oxalate is known to affect luminescence quenching.[5a,6,8] Its effect is depicted in Scheme 3, where $Ru(bpy)_3^{3+}|X^-$ denotes the ion pair complex and K_{ip} is the ion pair formation constant. Ion

SCHEME 3

$$Ru(bpy)_3^{3+} + C_2O_4^{2-} \rightleftarrows Ru(bpy)_3^{3+}|C_2O_4^{2-} \qquad K_{ip} \quad (ip)$$

$$Ru(bpy)_3^{3+}|C_2O_4^{2-} \xrightarrow{k_0} Ru(bpy)_3^{2+}|C_2O_4^{\bullet-} \quad (0ip)$$

$$Ru(bpy)_3^{2+}|C_2O_4^{\bullet-} \longrightarrow Ru(bpy)_3^{2+} + C_2O_4^{\bullet-}$$

$$C_2O_4^{\bullet-} \xrightarrow{k_1} CO_2 + CO_2^{\bullet-} \quad (1)$$

$$Ru(bpy)_3^{3+} + CO_2^{\bullet-} \xrightarrow{k_2} Ru(bpy)_3^{2+} + CO_2 \quad (2)$$

pair formation can be quantitatively described by an electrostatic model first developed by Fuoss.[21,23] In this model, eqs 12−14, K_{ip} is a function of the ionic strength.

$$K_{ip} = \frac{4\pi N\sigma^3}{3000}\exp(-w(\sigma,\mu)/kT) \quad (12)$$

$$w(\sigma,\mu) = \frac{Z_1Z_2e^2}{\epsilon\sigma(1+\beta\sigma\mu^{1/2})} \quad (13)$$

$$\beta = \left(\frac{8\pi N_A e^-}{1000\epsilon kT}\right)^{1/2} \quad (14)$$

where ϵ is the solvent dielectric constant, μ is the ionic strength, Z_1 and Z_2 are the charges of the ions involved in the ion pair, and σ is the distance of closest approach, taken as the sum of the hard-sphere radii for $Ru(bpy)_3^{2+}$ (6.8 Å)[21a,24,25] and for $C_2O_4^{2-}$ (assumed to be 2.0 Å[26]). All of the other terms have their usual meanings.

Note that this model does not take into account specific ion effects that are frequently observed with Ru complexes.[27] Typically, our results also reflect such effects because at the same ionic strength $\mu = 0.4$ M, the homogeneous ET rate constant obtained in Na_2SO_4 solution ($k_{0obs} = 1.2 \times 10^4\ M^{-1}\ s^{-1}$) is lower than the value obtained in a NaCl/phosphate buffer solutions ($k_{0obs} = 1.4 \times 10^4\ M^{-1}\ s^{-1}$). No attempt was made to investigate these ion-specific effects further.

If one considers Scheme 3 for the homogeneous oxidation of oxalate, the observed rate constant should be given by eq 15:

$$k_{0obs} = \frac{k_0K_{ip}[C_2O_4^{2-}]}{1 + \sum K_{ip}{}^i[A^i]} \quad (15)$$

where $[A^i]$ and $K_{ip}{}^i$ are, respectively, the concentration and the ion-pairing constant for the anion *i*. To a first approximation, the ion-pairing constant has been considered identical to the value for oxalate for all of the anions present in the medium.[28] An average value of the ET within the ion pair rate constant $k = 3.2 \pm 0.2 \times 10^3\ s^{-1}$ has been determined using the experimental values of the observed rate constant k_{0obs} and the calculated ion-pairing constant K_{ip}. The agreement over the whole range of concentrations is depicted by the theoretical line in Figure 5. The good fit validates the reaction scheme and the data treatment.

Driving Force Influence on the Electron-Transfer Rate. The homogeneous oxalate oxidation was studied for a number of different tris(polypyridine)ruthenium(II) and -iron(II) complexes. The electrochemical characteristics obtained from cyclic voltammograms of these complexes are listed in Table 1. They

TABLE 1: Homogeneous Oxidation of the Oxalate Dianion

complex	E^0, V vs NHE[a]	$D_{P/Q}$ ($\times 10^6$ cm^2 s^{-1})[b]	k (s^{-1})[c]
$Ru(bpy)_3^{2+}$	1.26	5.9	2.9×10^3
$Ru(phen)_3^{2+}$	1.25_5	5.7	2.0×10^3
$Ru(bpy)_2(dmbp)^{2+}$	1.21	5.3	7.4×10^2
$Ru(dmphen)_3^{2+}$	1.12	4.3	1.7×10^2
$Ru(dmbp)_3^{2+}$	1.10	4.4	80
$Fe(bpy)_3^{2+}$	1.05_5	4.3	20
$Fe(dmbp)_3^{2+}$	0.92_5	3.7	0.90

[a] E^0, standard oxidation potentials (vs NHE) for the different redox couples investigated in 0.1 M NaCl + 0.1 M phosphate buffer, pH 6.1, at 20 °C. [b] $D_{P/Q}$, diffusion coefficient. [c] k, electron-transfer rate constants within the ion pair.

are denoted as RuL_3^{2+} and FeL_3^{2+}, where L = 2,2′-bipyridine (bpy), 4,4′-dimethyl-2,2′-bipyridine (dmbp), 9,10-phenanthroline (phen), 4,7-dimethyl-9,10-phenanthroline (dmphen), and $Ru(bpy)_2(dmbp)^{2+}$. Because the ET rate constants are obtained by electrochemical means, the solubility of the chosen redox mediators had to be greater than 0.1 mM to be easily detected. This is the case for all the mediators investigated. The standard oxidation potentials of the mediators listed in Table 1 are in good agreement with the values previously reported.[21d]

In all cases, the catalytic efficiency i_s/i_{s0} varied linearly with the square root of the oxalate concentration (Figure 2), but was independent of the mediator concentration. This observation indicates that, as for $Ru(bpy)_3^{2+}$, the process is kinetically controlled by the homogeneous ET. The homogeneous ET rate constants, k, were extracted from the redox catalysis experiments, as previously described. To treat the ET within the ion pair, we assumed the same ion pair effect for all of these redox couples because they all involve 3+ and 2+ charges, have, to a first approximation, similar sizes, and were all studied in the same NaCl/phosphate buffer solution (pH = 6.1). We calculated the rate constant within the ion pair using the following equation:

$$k_{ML_3^{2+}} = k_{0obs,ML_3^{2+}} \frac{k_{Ru(bpy)_3^{2+}}}{k_{0obs,Ru(bpy)_3^{2+}}} \qquad (16)$$

where k_X and $k_{0obs,X}$ denote respectively the rate constant for the X complex observed within the ion pair and in solution.

The values of the rate constant for the ET to the oxalate dianion within the ion pair are gathered in Table 1. Obviously, the higher the oxidation potential, the faster the ET. Before the rationalization of these data in terms of structure−activity relationships is presented, the influence of all the studied parameters on the ECL process will be described.

Electrogenerated Chemiluminescence. ECL can be generated by oxidation of $Ru(bpy)_3^{2+}$ in the presence of different coreactants (oxalate and other carboxylates,[2] trialkylamines,[29] triphenylphosphine,[29a] and reduction of $Ru(bpy)_3^{2+}$ in the presence of peroxydisulfate in acetonitrile[30]). This ECL can be explained by the reactions in Scheme 4.

In acetonitrile, oxalate has been shown to be easier to oxidize than the $Ru(bpy)_3^{2+}$ complex.[31] Thus, both reactants are oxidized at the electrode during light generation. The short-lived oxalate radical anion is then transformed into the carbon dioxide radical anion close to the electrode, where most of it is oxidized. The main undesirable effects of the direct oxidation are possible side reactions at the electrode surface and a substantial loss of the reducing intermediate for the ECL generation.

However, in aqueous solution, the oxalate species are only oxidized via solution reactions 0, 1, and 2, or 2*, or 17 and 18. $CO_2^{\bullet-}$ is then produced and oxidized far from the electrode. Its formation rate and consequently the ECL emission should depend on the homogeneous redox catalysis process. Figure 6 shows the ECL intensity, I_l, recorded as a function of the electrode potential, E. In the absence of oxalate, the light intensity is at the noise level. When 1 mM oxalate is added to the solution, light is generated when $Ru(bpy)_3^{2+}$ is oxidized at the electrode. The light intensity profile I_l-E follows the anodic current; it has the same sigmoidal shape and attainment of a steady light intensity plateau. An increase in the oxalate concentration increases both the steady current and light intensity. Figure 7 is a summary of the data, showing that the catalytic efficiency (i_s/i_{s0}) varies linearly with the plateau light intensity, I_{ls}, normalized by the initial ruthenium concentration ($I_{ls}/[Ru^{2+}]^0$).

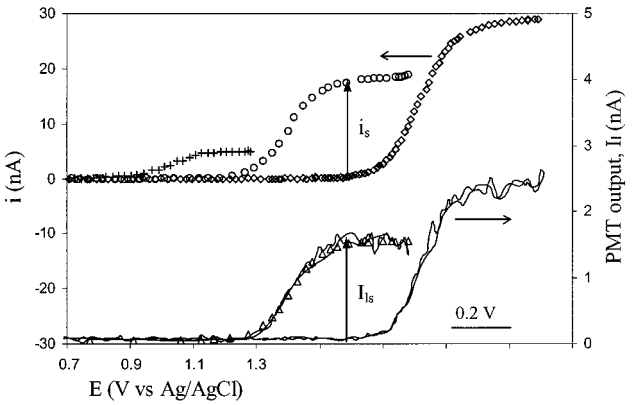

Figure 6. Current−potential and light intensity−potential curves for 1 mM $Ru(bpy)_3^{2+}$ and, from left to right, 0, 1, and 2 mM $C_2O_4^{2-}$ in 0.1 M NaCl + 0.1 M phosphate buffer, pH = 6.1, at a 50-μm diameter Pt ultramicroelectrode; scan rate, 10 mV/s. Upper: current, i, with the curves for 1 and 2 mM $C_2O_4^{2-}$ shifted by 0.4 and 0.8 V, respectively, for clarity. Lower: light intensities, I_l, (—) experimental and (△) simulated curves according to eq 10.

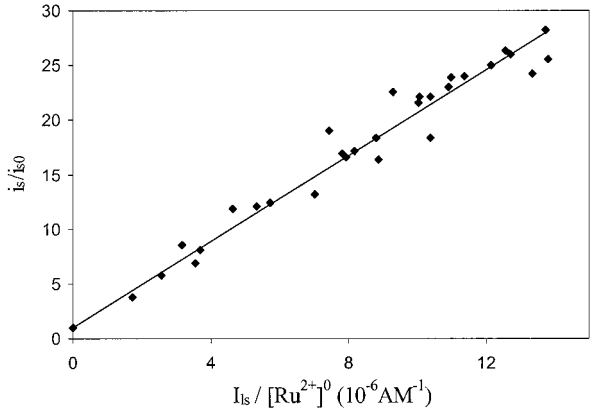

Figure 7. Variation of the normalized catalytic current, i_s/i_{s0}, with the normalized plateau light intensity, $I_{ls}/[Ru^{2+}]$, for $0.4 < [Ru(bpy)_3^{2+}] < 4$ mM and $1 < [C_2O_4^{2-}] < 30$ mM in 0.1 M NaCl + 0.1 phosphate buffer, pH = 6.1.

SCHEME 4

$$Ru(bpy)_3^{3+} + CO_2^{\bullet-} \xrightarrow{k_2} Ru(bpy)_3^{2+} + CO_2 \qquad (2)$$

$$Ru(bpy)_3^{3+} + CO_2^{\bullet-} \xrightarrow{k_{2^*}} Ru(bpy)_3^{2+*} + CO_2 \qquad (2^*)$$

$$Ru(bpy)_3^{2+} + CO_2^{\bullet-} \xrightarrow{k_{17}} Ru(bpy)_3^{+} + CO_2 \qquad (17)$$

$$Ru(bpy)_3^{3+} + Ru(bpy)_3^{+} \xrightarrow{k_{18}} Ru(bpy)_3^{2+*} + Ru(bpy)_3^{2+} \qquad (18)$$

TABLE 2: Summary of the Rate Constants of the Competing Oxidation Routes of $CO_2^{\bullet-}$

reaction	E^0_{Ru} (V vs NHE)	ΔG_0 (eV)	w_r (eV)[b]	k (M^{-1} s^{-1})[c]
$Ru(bpy)_3^{3+} + CO_2^{\bullet-} \rightarrow Ru(bpy)_3^{2+} + CO_2$	1.26	−3.16	−0.03	5.2×10^9
$Ru(bpy)_3^{3+} + CO_2^{\bullet-} \rightarrow Ru(bpy)_3^{2+*} + CO_2$	−0.84[a]	−1.06	−0.03	5.4×10^9
$Ru(bpy)_3^{2+} + CO_2^{\bullet-} \rightarrow Ru(bpy)_3^{+} + CO_2$	−1.28[a]	−0.62	−0.02	7×10^7

[a] From ref 21. [b] Calculated using eq 13 with radii of $CO_2^{\bullet-}$, 0.80 Å,[44b] RuL_3, 6.8 Å and with $\mu = 0.4$ M and $T = 20$ °C. [c] Calculated from eqs 30 and 37 using the parameters defined in ref 44; see text.

TABLE 3: Estimation of the ECL Quantum Efficiencies for the Different $RuL'L_2^{2+}$ Species in Aqueous Solution at 20 °C

complex	β	$E^0_{3+/2+}$ (V vs NHE)	$E^0_{3+/2+*}$[a] (V vs NHE)	k_2[b] (10^{-9} M^{-1} s^{-1})	$k_2{}^*$[b] (10^{-9} M^{-1} s^{-1})	η_2	η_r	$\eta = \eta_r\eta_2/2$[c]
$Ru(bpy)_3$	0.097	1.26	−0.84	5.2	5.4	0.51	0.042[d]	1.1×10^{-2}
$Ru(phen)_3$	0.14	1.25_5	-0.87_5	5.4	4.6	0.46	0.06_5[e]	1.5×10^{-2}
$Ru(bpy)_2dmbp$	0.044	1.21	−0.88	6.5	4.3	0.40	0.025[d]	5.0×10^{-3}
$Ru(dmbp)_3$	0.012	1.10	−0.94	8.8	2.8	0.24	0.014[d]	1.7×10^{-3}
$Ru(dmphen)_3$	0.084	1.12	−0.98	8.4	2.0	0.19	−	−

[a] Calculated from $E^0_{3+/2+*} = E^0_{3+/2+} - E_{em}$ where E_{em} is the emission energy of the Ru^{2+}* complex, E_{em} taken from refs 21a,d and 48a. [b] Calculated from eqs 30 and 37, using $\Delta G^{\neq}_0 = 0.52$ eV; see text. [c] $\eta_2 = k_2^*/(k_2 + k_2^*)$. [d] Refs 48a,b. [e] Refs 48a,c.

We now will correlate the electrochemical and ECL results and discuss the mechanism of the ECL process. Previous studies addressed the mechanism of ECL for the $Ru(bpy)_3^{2+}$/oxalate system. When an electrode is covered by a Nafion film containing $Ru(bpy)_3^{2+}$ and placed in an oxalate solution, the light intensity can be qualitatively simulated[2b] using the formalism developed by Feldberg for the annihilation reaction.[32] More recently, the current−light intensity dependences observed during ECL experiments under sonication were rationalized by a simple quadratic expression.[33]

Although $Ru(bpy)_3^{+}$ is unstable in aqueous solution,[2a] the light production may arise from oxidation of the carbon dioxide radical anion by both $Ru(bpy)_3^{2+}$ and $Ru(bpy)_3^{3+}$ (eqs 2* and 18). The former equation was shown to be more favorable in acetonitrile.[31] Because we used ultramicroelectrodes that provide steady-state mass transport, we treat the system with the assumption that every reaction is at steady state, i.e., there is no accumulation of intermediates. The steady-state light intensity, I_{ls}, is then proportional to the rate of radiative decay of $Ru(bpy)_3^{2+}$*,

$$I_{ls} = \alpha k_r[Ru^{2+*}] \tag{19}$$

where k_r is the rate constant for the radiative decay of the excited state, represented as Ru^{2+}*. The other species, $Ru(bpy)_3^{+}$, $Ru(bpy)_3^{2+}$, and $Ru(bpy)_3^{3+}$, are denoted Ru^+, Ru^{2+}, and Ru^{3+}, respectively, and α is a proportionality constant. The different species concentrations can be expressed using the steady-state assumption by

$$\partial[Ru^{2+*}]/\partial t = 0 = k_{18}[Ru^+][Ru^{3+}] + k_{2*}[Ru^{3+}][CO_2^{\bullet-}] - (k_r + k_{nr})[Ru^{2+*}] \tag{20}$$

where k_{nr} is the nonradiative decay rate constant of Ru^{2+}*, which can be related to the luminescence quantum yield, η_r, and to the Ru^{2+*} lifetime, τ, by

$$\eta_r = k_r/(k_r+k_{nr}) = k_r\tau \tag{21}$$

$$\partial[Ru^+]/\partial t = 0 = k_{17}[Ru^{2+}][CO_2^{\bullet-}] - k_{18}[Ru^+][Ru^{3+}] \tag{22}$$

$$\partial[CO_2^{\bullet-}]/\partial t = 0 = k_0[Ox][Ru^{3+}] - (k_{17}[Ru^{2+}] + (k_2 + k_{2*})[Ru^{3+}])[CO_2^{\bullet-}] \tag{23}$$

These equations yield the concentrations of $[CO_2^{\bullet-}]$ and $[Ru^{2+}*]$ as a function of k_0, [Ox], $[Ru^{3+}]$, and $[Ru^{2+}]$. If we assume no accumulation of Ru^{3+} in the reaction layer, we can then relate its concentration to the plateau current magnitudes for Ru^{2+} oxidation in the presence and the absence of oxalate, i_s and i_{s0}, respectively,[34] by

$$\partial[Ru^{3+}]/\partial t = 0 = (i_s - i_{s0})/F\upsilon - 2k_0[Ox][Ru^{3+}] \tag{24}$$

Note that all of these reactions should be faster than the first ET, which remains as the rate-determining step. Moreover, because of the steady-state assumption, any different paths for the decay of $CO_2^{\bullet-}$ or the intervention of other ruthenium intermediates do not alter the previous kinetic analysis so that the diffusion equation for Ru^{3+} and the data treatment hold. Combining eqs 19−24 thus yields

$$I_{1s} = \alpha' \frac{k_r}{k_r + k_{nr}}(i_s - i_{s0})\frac{k_{2*}[Ru^{3+}] + k_{17}[Ru^{2+}]}{(k_{2*} + k_2)[Ru^{3+}] + k_{17}[Ru^{2+}]} \tag{25}$$

where α' is a constant that depends on the PMT efficiency and on the light collection geometry of the system. A simpler form can be obtained if one makes further assumptions related to the large difference in the driving forces of reactions 2, 2*, and 17 ($\Delta G^0_2 < \Delta G^0_{2*} < \Delta G^0_{17}$ from the values reported in Table 2). Two limiting situations can be predicted according to the competition between these three steps.

If eq 2 is in the inverted region, one may assume $k_2 \ll k_{2*}$ and k_{17} and neglect reaction 2 over (2*) and (17). Then, eq 25 becomes

$$I_{ls} = \alpha' \frac{k_r}{k_r + k_{nr}}(i_s - i_{s0}) = \beta(i_s - i_{s0}) \tag{26a}$$

If eq 2 is not in the inverted region, then neither will be eq 2* nor eq 17. The rate of eq 17 should be negligible compared to eqs 2* and 2. Equation 25 then becomes

$$I_{ls} = \alpha' \frac{k_r}{k_r + k_{nr}}\frac{k_{2*}}{k_{2*} + k_2}(i_s - i_{s0}) = \beta(i_s - i_{s0}) \tag{26b}$$

where β is used throughout to represent $I_{1s}/(i_s - i_{s0})$.

It is noteworthy that in both cases I_{ls} varies linearly with the catalytic plateau current, i_s. Within experimental accuracy, eq 26 fits with the experimental results quite well, which supports the simple model.

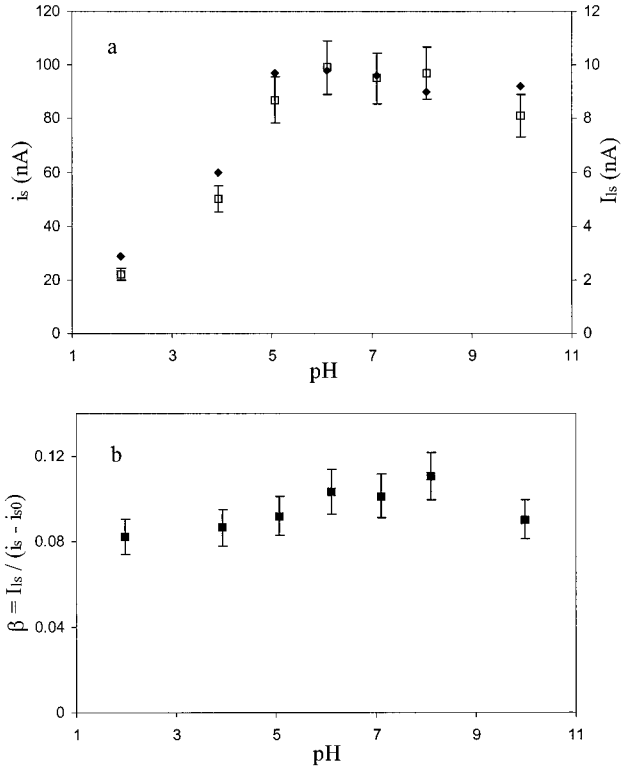

Figure 8. (a) Variation of the plateau (□) light, I_{ls}, and (◆) current, i_s, intensities with pH. $[Ru(bpy)_3^{2+}] = 0.75$ mM and $[C_2O_4^{2-}] = 30$ mM in 0.1 M NaCl + 0.1 M phosphate buffer, except for pH 1.2 (0.15 M H_3PO_4). (b) Variation of β with the pH. $0.5 < [Ru(bpy)_3^{2+}] < 0.9$ mM and $10 < [C_2O_4^{2-}] < 40$ mM.

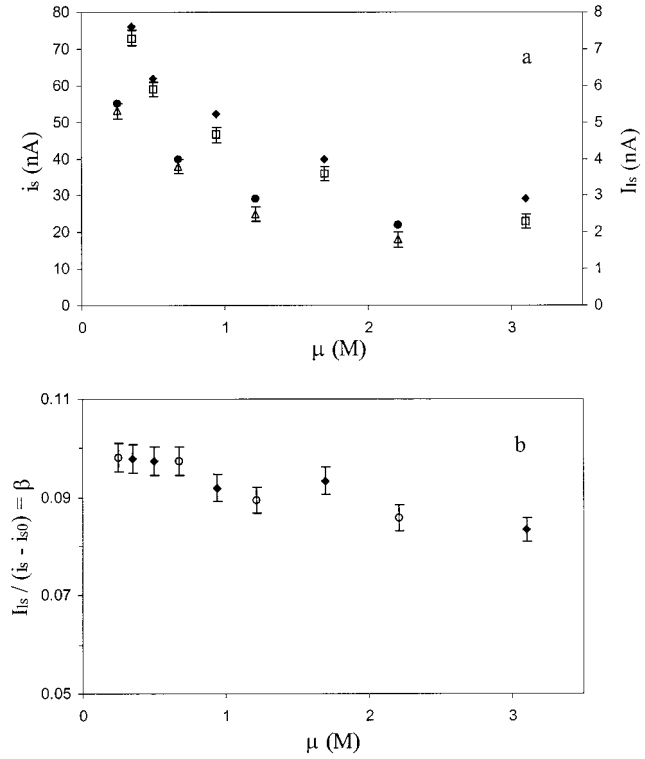

Figure 9. (a) Variation of the plateau (□, △) light, I_{ls}, and (●, ◆) current, i_s, intensities with the ionic strength, μ. $[Ru(bpy)_3^{2+}] =$ (△, ●) 0.3 and (□, ◆) 0.5 mM; $[C_2O_4^{2-}] =$ (△, ●) 21 and (□, ◆) 30 mM in Na_2SO_4 solutions. (b) Variation of β with the ionic strength, μ: $[Ru(bpy)_3^{2+}] =$ (○) 0.3 and (◆) 0.5 mM; $[C_2O_4^{2-}] =$ (○) 21 and (◆) 30 mM in Na_2SO_4 solutions.

When oxalate is in excess, one can combine eqs 6 and 26 to give the variation of the normalized light intensity with the initial oxalate concentration $[Ox]^0$ and the homogeneous ET rate constant k_0:

$$I_{ls} = \beta' \left(\frac{2k_0[Ox]^0}{D}\right)^{1/2} i_{s0} \qquad (27)$$

This equation indicates the extent to which the ET affects the ECL emission. The linear relationship between I_{ls} and i_s also rationalizes the shape of the light profile. In fact, the voltammogram defined in eq 10 can also be applied to describe, with quite good agreement, the light emission (dashed line in Figure 7).

The variation of the light and current intensities with the pH are indicated in Figure 8a. For pH > 8, the ECL intensity I_l tends to decrease with increasing positive UME bias after reaching a maximum. Because the reverse scan superimposes on the forward one, the reversible decrease in light intensity can be attributed to an increase in the rate of oxygen evolution, which is shifted more negatively and thus becomes more important when the pH increases. A more positive potential will result in an apparent lowering in the light intensity, as was seen in previous studies.[2a] The value of I_{ls} used in Figure 8a is then the maximum light intensity observed on the I_l-E curve.

As previously reported,[2a] I_{ls} strongly depends on the pH, but clearly follows changes of the steady current i_s. The variation of the proportionality factor β with pH (Figure 8b) shows that β is largely independent of pH. The decrease observed for pH > 8 can be attributed to the increasing importance of oxygen evolution. For pH < 4, the slightly lower efficiency could be due to the intervention of direct oxalic acid oxidation. Overall, these effects are minor and the ECL efficiency is not affected by more than 20% by a change in pH. These results emphasize the idea that the light emission is, to a first approximation, simply governed by the first homogeneous ET.

Similarly, the ionic strength has a small influence on the light generation. Figure 9 shows the different steady light, I_{ls}, and current, i_s, intensities for different solutions containing the same $Ru(bpy)_3^{2+}$ and oxalate concentrations but different ionic strengths (adjusted with Na_2SO_4). The effect of ionic strength corresponds to the variation predicted by eq 15: the lower the ionic strength, the faster the homogeneous ET and the higher the steady light and current intensities. The variation of β with the ionic strength is not really clear, but seems to decrease slightly when the ionic strength is increased, indicating a decrease in the ECL efficiency with increasing ionic strength. This observation might be connected with the effect of ionic strength on the photoluminescent quantum yield.

To emphasize the importance of the homogeneous ET in the overall process, we investigated ECL generation for different ruthenium species $RuL'L_2^{2+}$, varying the driving force of the homogeneous ET. The light intensity profiles observed for all the Ru complexes, except the phenanthroline one, showed a sigmoidal shape and steady light intensity. In the case of the phenanthroline complex, the light intensity reached a maximum and then decreased with increasing potential. During the reverse scan, the light intensity reached a second maximum, but lower than the maximum found on the forward scan; the voltammogram does not indicate any current decay. This behavior can be attributed to degradation of the excited ruthenium complex, forming an intermediate that could be oxidized (explaining the steady current) but could not generate excited states. For this complex, the maximum in light intensity was taken as the value of I_{ls}.

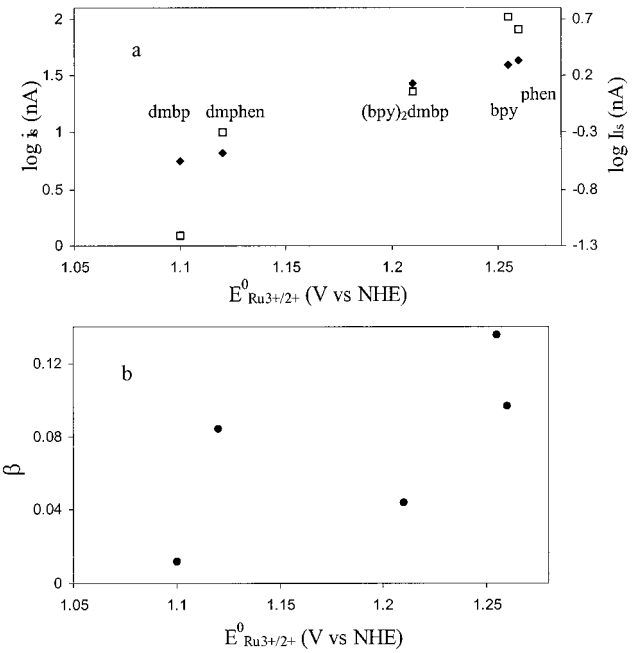

Figure 10. (a) Variation of the logarithm of the plateau (□) light, I_{ls}, and (◆) current, i_s, intensities with the standard oxidation potential of $RuL'L_2^{2+}$. $[RuL'L_2^{2+}] \approx 0.25$ mM and $[C_2O_4^{2-}] = 50$ mM in 0.1 M NaCl + 0.1 M phosphate buffer, pH 6.1. (b) Variation of β with the standard oxidation potential of $RuL'L_2^{2+}$. $0.15 < [RuL'L_2^{2+}] < 0.25$ mM and $10 < [C_2O_4^{2-}] < 30$ mM. From left to right, $RuL'L_2^{3+} = Ru(dmbp)_3^{2+}$, $Ru(dmphen)_3^{2+}$, $Ru(dmbp)(bpy)_2^{2+}$, $Ru(phen)_3^{2+}$, and $Ru(bpy)_3^{2+}$.

A plot of the logarithm of the steady or maximum current, i_s, and light, I_{ls}, intensities obtained during the catalytic oxalate oxidation by the Ru complexes as a function of the potential of the complex (Figure 10a) shows that a larger driving force results in a faster homogeneous ET and higher current and light intensities. Previous attempts to correlate the ET driving force of the first oxidation step to the light intensity have been reported in the literature. Qualitative results were mentioned for ECL generated with Rh complexes in the presence of coreactants.[35] More quantitatively, a linear relationship was observed between the logarithm of the light intensity obtained for different coreactant/$Ru(bpy)_3^{2+}$ systems and the coreactant ionization potential,[29a] the latter taken as being proportional to the coreactant redox potential. Equation 27 allows one to correlate the light intensity with k, the homogeneous ET rate constant. As will be shown in the next section, this k depends on both the coreactant and RuL_3^{2+} oxidation potentials and increases with the driving force of the initial reaction. However, the parameter β, defined by eq 26, fluctuated considerably with different ligands in the Ru complexes (Figure 10b). This variation can reflect differences in the luminescence processes (eq 21) and in the competition for $CO_2^{\bullet-}$ oxidation (eq 26). Although this effect is significant, to a first approximation, the light emission simply reflects the efficiency of the catalytic oxalate oxidation and can be understood in terms of differences in the ET rate constant with the redox couple.

Application of Electron-Transfer Theory to Electron-Transfer Rates. One may attempt to use the Marcus theory to correlate the observed variation in the ET rate constant to variations in the driving force. Generally, the observed rate constant takes into account both the true activation processes: formation of a precursor complex and dissociation of the successor complex (Scheme 5). Note that the rate constants

SCHEME 5

$$\begin{array}{ccc} Ru(bpy)_3^{3+} + C_2O_4^{2-} & \xrightleftharpoons{\Delta G_0} & Ru(bpy)_3^{2+} + C_2O_4^{\bullet-} \\ \uparrow\downarrow w_r & & \uparrow\downarrow w_p \\ Ru(bpy)_3^{3+}\,|\,C_2O_4^{2-} & \xrightleftharpoons{\Delta G'_0} & Ru(bpy)_3^{2+}\,|\,C_2O_4^{\bullet-} \end{array}$$

extracted from our experiments describe the ET within the ion pair and take into account precursor complex formation.

Because the formation and dissociation processes generally occur at the diffusion limit, the measured ET rate constants are the rate constants for the pure activation process. Nevertheless, the free energy to which they are related is given by

$$\Delta G_0' = \Delta G_0 + w_p - w_r = E^0_{Ox} - E^0_{Q/P} + w_p - w_r \quad (28)$$

where w_r and w_p represent, respectively, the reactants and the product work terms. These are generally estimated by the electrostatic model given by the Fuoss−Eigen equation.[21,23]

The free energy of activation, $\Delta G^{\neq}$, for ET within the ion pair is evaluated from the rate constant k by

$$\Delta G^{\neq} = -RT/F \ln(k/\nu_n) \quad (29)$$

where ν_n is a vibration frequency, taken to be 10^{11} s^{-1}. The Marcus equation relates the activation free energy to the driving force change $\Delta G_0'$ and the intrinsic activation energy $\Delta G_0^{\neq}$.

$$\Delta G^{\neq} = \Delta G_0^{\neq}\left(1 + \frac{\Delta G_0'}{4\Delta G_0^{\neq}}\right) \quad (30)$$

The latter can be described in terms of reorganization energy, $\Delta G_0^{\neq} = \lambda/4$, as the contribution of two terms, λ_i, the internal reorganization energy and the solvation reorganization energy, λ_0. Because the oxalate dianion is relatively small compared to the different redox couples used,[28b] most of the reorganization contribution comes from changes in solvation, evaluated from

$$\lambda_0 = e^2\left(\frac{1}{n^2} - \frac{1}{D_s}\right)\left(\frac{1}{2a_M} + \frac{1}{2a_{Ox}} - \frac{1}{\sigma}\right) \quad (31)$$

Different empirical equations of the form of eq 32 have been proposed for the evaluation of the solvent reorganization energy.

$$\lambda_0 \approx A\left(\frac{1}{a_M} + \frac{1}{a_{Ox}} - \frac{2}{\sigma}\right) \quad (32)$$

where A can be 3.2[36] or 3.8 eV[21a] when the hard-sphere radii are expressed in Å. Taking $a_M \approx a_{Fe} \approx a_{Ru} \approx 6.8$ Å, $a_{Ox} = 2$ Å, and $\sigma \approx a_M + a_{Ox}$, one obtains $\lambda_0 \approx 0.34-0.40$ eV.

We mentioned that oxalate could be oxidized according to a dissociative ET (inner-sphere ET). The simple Marcus model does not describe a dissociative ET because the products cannot be depicted by the harmonic oscillator approximation. Using a Morse description, Savéant extended the Marcus theory to include the dissociative case[4] and showed that the activation−driving force relationship was still quadratic (eq 30). The intrinsic activation free energy contains, in addition to the reorganization terms defined by Marcus, one-fourth of the homolytic dissociation energy of the substrate, denoted D_{Ox}, and $\Delta G^{\neq}_0 = \lambda/4 + D_{Ox}/4$. The oxalate bond dissociation energy should be approximately in the range of the value determined for oxalic acid, $D_{Ox} \approx D_{C_2O_4H_2} = 2.87$ eV.[20,37] Moreover, the driving force expression now includes the standard oxidation

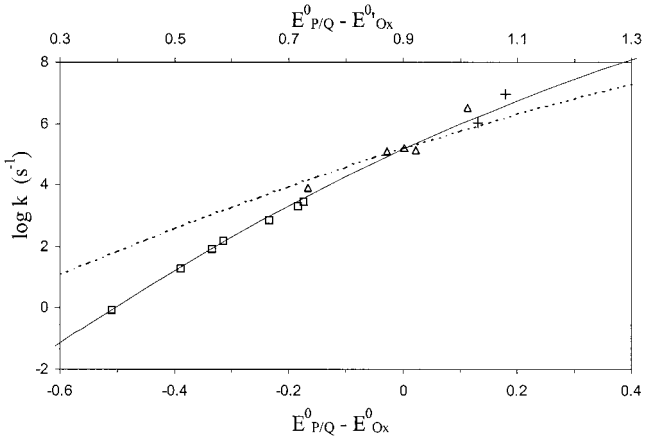

Figure 11. Variation of the logarithm of the electron-transfer rate constant within the ion pair, log k, with ($E^0_{Q/P} - E^0_{Ox}$) or ($E^0_{Q/P} - E^{0\prime}_{Ox}$) for outer-sphere and dissociative electron transfer, respectively; (□) this work, (△) from ref 6, (+) from ref 8, theoretical simulations according to (—) Marcus equation, and (- - -) Savéant equation.

potential of the dissociative ET $E^0_{CO_2^{\bullet-}+CO_2/C_2O_4^{2-}}$, instead of $E^0_{Ox} = E^0_{C_2O_4^{\bullet-}/C_2O_4^{2-}}$.

We consider not only the ET rate constants obtained from our redox catalysis experiments but also those derived from luminescence quenching by oxalate of different excited states of CrL_3^{3+*} [6] or $RuL'_2L''^{2+*}$ [8] (where L is a substituted 2,2′-bpyridine or phenanthroline, L′ is the 2,2′-bpyrazine, and L″ is L′ or the 2,2′-bpyrimidine). As the ion-pairing formation has been taken into account by the authors in the case of the luminescence quenching of the Cr^{3+*} exited state, their data were used without modification. In the case of the Ru^{2+*} excited-state quenching, ion pairing was mentioned but not taken into account. According to the experimental conditions ($\mu = 1$ M), one predicts, using eq 12, an ion pair equilibrium constant of 4 M^{-1}. The ET rate constant within the ion pair can then be estimated by the same formalism $k = k_{0obs}(1 + K[SO_4^{2-}])/K = k_{0obs}/1.8$. The product work terms are estimated by eq 13 as $w_r - w_p = -15$ mV for both systems.

Figure 11 shows the variation of the logarithm of k_0, the experimental ET rate constant within the ion pair, with the ET driving force and a fit to these variations by both the Marcus and Savéant equations. Note that, in the case of the Savéant model, the intrinsic activation energy should be at least $D/4 = 0.72$ eV. This minimum value for the dissociative ET description yields the dashed line in Figure 11. The lack of a good fit of the experimental data with the Savéant equation suggests that the ET does not proceed by a dissociative path. The outer-sphere ET model fits better and it was possible to fit the complete set of data extracted from this work and from the luminescence quenching experiments (line in Figure 11) with values of the intrinsic barrier, $\Delta G_0^{\neq} = 0.34$ eV, and of an oxalate standard one-electron potential, $E^0_{Ox} = E^0_{C_2O_4^{\bullet-}/C_2O_4^{2-}} = 1.41$ V vs NHE. The intrinsic activation energy is in quite good agreement with values predicted by the empirical equation (eq 32). Moreover, even if one expects that electrostatic repulsion causes the bond dissociation energy of the oxalate dianion to be weaker than that for oxalic acid, the value of the intrinsic activation energy found here is clearly too small to account for both $^1/_4$ of the bond dissociation energy and the solvent reorganization energies and could not depict a dissociative mechanism. The standard oxidation potential is significantly higher than the previously reported value of 0.55 V,[2b] but closer to the more reasonable 1.7 V assumed from luminescence quenching experiments.[8]

Second-Electron Transfer. The first outer-sphere ET, discussed above, is then followed by the fragmentation of the oxalate radical anion. We could not extract the lifetime of this intermediate from these experiments. However, because the redox catalysis is kinetically controlled by the first ET, one can assume that the bond cleavage reaction, k_1, is faster than the back electron-transfer reaction so that $k_1 > k_{-0}[P]^0$. Knowledge of the standard potential for oxalate oxidation allows the determination of k_{-0} and then the minimum value of k_1. For the least-positive couple, $Fe(dmbp)_3^{2+}$, the back electron transfer is at the diffusion-controlled limit $k_{-0} = k_D = 3 \times 10^9$ M^{-1} s^{-1},[38] and then $k_1 > k_D[P]^0 = 6 \times 10^5$ s^{-1}, under our experimental conditions. Moreover, knowledge of the standard oxidation potential for the two-electron oxalate oxidation, $E^0_{2CO_2/C_2O_4^{2-}} = -0.55$ V vs NHE,[39] allows the estimation of ΔG^0_1,the free energy of the fragmentation reaction (eq 1), as $\Delta G^0_1 = 2E^0_{2CO_2/C_2O_4^{2-}} - E^0_{C_2O_4^{\bullet-}/C_2O_4^{2-}} - E^0_{CO_2/CO_2^{\bullet-}} = -0.61$ eV and $K_1 = 3 \times 10^{10}$ M^{-1}.

The carbon dioxide radical anion, $CO_2^{\bullet-}$, produced from $C_2O_4^{\bullet-}$ fragmentation, is a strong reductant ($E^0_{CO_2/CO_2^{\bullet-}} = -1.9$ V vs NHE[14]). Its reactivity has been explored. When generated by electrochemical reduction,[40] different paths were reported in acetonitrile. In the systems discussed here, $CO_2^{\bullet-}$ could decay by

(i) *oxidation by both RuL_3^{3+} and RuL_3^{2+} presented in Scheme 4.* The former leads to the formation of RuL_3^{2+} either in the ground (eq 2) or excited state (eq 2*). The latter generates RuL_3^{+} (eq 17), which will give rise, by a subsequent annihilation reaction with RuL_3^{3+} (eq 18), to the excited-state RuL_3^{2+*}.[41]

(ii) *an acid−base reaction.* The radical issuing from this protonation (eq 33) is still a sufficiently strong reductant to be involved in the same kind of redox reactions as in (i).

$$H_2O + CO_2^{\bullet-} \xrightarrow{k_{33}} HCO_2^{\bullet} + HO^- \qquad (33)$$

Because of the strong acidity of $HCO_2^{\bullet}$ ($pK_a = 1.4$[37]), its formation is probably negligible in the slightly alkaline medium. An estimate of its formation rate constant can be obtained by extrapolation of the estimated value in acetonitrile, $k = 7.7 \times 10^2$ M^{-1} s^{-1},[40a] to pure water $k_{33} = 4 \times 10^4$ s^{-1}.

(iii) *dimerization (eq 34), regenerating oxalate.* This is the main path in acetonitrile, but is negligible in water.[40]

$$CO_2^{\bullet-} + CO_2^{\bullet-} \xrightarrow{k_{34}} C_2O_4^{2-} \qquad (34)$$

We can get some idea of the rate constant of the bimolecular reactions of $CO_2^{\bullet-}$ with the different Ru species because the oxidation of $CO_2^{\bullet-}$ by different coordination complexes in aqueous solution has been investigated.[42−44] Marcus theory has been applied to explain the rate of $CO_2^{\bullet-}$ oxidation by different cobalt complexes.[42] The very large ET barrier found for the $CO_2/CO_2^{\bullet-}$ couple ($\Delta G^{\neq}_0 \approx 0.9$ eV) was attributed to geometry changes when passing from the bent $CO_2^{\bullet-}$ to the linear CO_2.[45] However, the uncertainties in the redox potentials render this value too imprecise to be used here. We preferred to use the results from measurements of the ET between different tris(polypyridine)ruthenium(II) and $CO_2^{\bullet-}$ (eq 35) obtained by pulse radiolysis.[44]

$$CO_2^{\bullet-} + RuLL'L''^{2+} \xrightarrow{k_{35}} CO_2 + RuLL'L''^{+} \qquad (35)$$

where L, L′, and L″ can be the 2,2′-bpyridine, 2,2′-bpyrazine, or the 2,2′bpyrimidine.

In this work, the authors showed that the ET was rationalized by the Marcus−Agmon−Levine empirical hyperbolic equation (eq 36);

$$\Delta G^{\neq} = \Delta G_0' + \frac{\Delta G^{\neq}_0}{\ln 2} \ln\left[1 + \exp\left(-\frac{\Delta G_0' \ln 2}{\Delta G^{\neq}_0}\right)\right] \quad (36)$$

where all the free energies have the meanings defined previously. This empirical equation, previously derived by Marcus for atom- and proton-transfer reactions, was preferred because the driving force range span was not very exothermic. However, this equation does not exhibit the Marcus inverted region and thus does not hold for highly energetic electron transfers, as encountered in ECL reactions. To rationalize our experiments, we thus treated the data from ref 44 with eq 30, rather than eq 36.

The expression of the experimentally observed rate constant k_{obs} is given by

$$1/k_{obs} = 1/k_D + 1/K_{ip}'k_{act} \quad (37)$$

where K_{ip}' is the formation constant of the $Ru^{2+}|CO_2^{\bullet-}$ ion pair given by eq 12 and k_{act}, the true activation rate constant within the ion pair, is given by the Marcus equation (eq 29). With the set of kinetic constants reported by the authors, $k_D = 1.1 \times 10^{10}$ M^{-1} s^{-1}, $k_{-D} = k_D/K_{ip}' = 3.7 \times 10^9$ M^{-1} s^{-1}, and $\nu_n = 6 \times 10^{12}$ s^{-1}, the radiolytic reduction rate constant of $RuLL'L''^{2+}$ is obtained using $\Delta G^{\neq}_0 = 0.52$ eV (instead of 0.59 eV using the Marcus−Agmon−Levine formalism). Note that the activation barrier is still large compared to that found in the case of oxalate oxidation, confirming the much larger reorganization energy. Our system deals with oxidative ET between the ruthenium species and $CO_2^{\bullet-}$, and as there is little change in structure when passing from the ruthenium(II) to its excited state or to the ruthenium(III) species,[46] we used the same set of parameters to estimate the rate constant for the various $CO_2^{\bullet-}$ oxidation routes described. These values are reported in Table 2. The work terms are calculated as previously described; w_p is negligible because CO_2 is uncharged, and we used a radius of 0.8 Å for $CO_2^{\bullet-}$ [44b] and 6.8 Å for the ruthenium species.

When L = bpy, the calculations predict that the main oxidation process is the formation of $Ru(bpy)_3^{2+}$ in the excited state (eq 2*), with a rate that is only slightly larger than that for the formation of the ground state (eq 2). While such exothermic reactions are in the Marcus inverted region for systems that are weakly solvated or require negligible reorganization, large values of λ can have a significant effect. Typically, the annihilation reaction (eq 18), which has an intrinsic activation energy of 0.2 eV, has been experimentally demonstrated to be in the Marcus-inverted region.[41,46] However, $CO_2^{\bullet-}$ is a much smaller molecule that requires significantly more solvation and internal reorganization. Because of the expected high activation barrier, the inverted region is shifted toward more exothermic values of the driving force, and the diffusion-controlled region expands over a wider range of driving forces (approximately 2.5 eV in the present case), explaining why eq 2 makes such a significant contribution. Equation 2* is a competitive route for the ET, explaining the ECL generation but also the low quantum efficiency compared to the annihilation route (eq 18).[2a] Reaction 17, $CO_2^{\bullet-}$ with $RuL'L_2^{2+}$, is greatly disfavored and can be neglected in a first approximation. Moreover, reactions 2 and 2* greatly predominate over the other routes envisaged.

Driving Force Influence on the ECL. With knowledge of the main reactions for the second ET to $CO_2^{\bullet-}$, it is possible to explain the differences observed in the ECL experiments for the different $RuL'L_2^{2+}$. To a first approximation, ECL generation is governed by the driving force of the first homogeneous ET. However, there are still large differences in the light emission observed when the ligands of the Ru species are changed. The dimensionless parameter, β, clearly confirms these differences. From the calculated values of the different competing oxidation paths of $CO_2^{\bullet-}$, eq 26b holds as the best description of the ECL process. Therefore, β, given by eq 26b, should reflect η, the quantum yield of the ECL process (Table 3). The latter can be defined as the product of the luminescence quantum efficiency, $\eta_r = k_r/(k_r + k_{nr})$, and the yield describing the competition between the ground-state and the excited-state formation, $\eta_2 = k_2^*/(k_2 + k_2^*)$. One may thus attempt to correlate the variation of β with the total quantum yield, $\eta = \eta_r\eta_2/2$.[47] The formalism adopted in the previous paragraph was applied to evaluate the different k_2 and k_2^* for each $RuL'L_2^{2+}$ and then η_2. The values of η_r were taken from the literature.[48] We could not find a value of η_r in aqueous solution for $Ru(dmphen)_3^{2+}$. For all of the other complexes, the variation of the ratio of the plateau or maximum light intensity, I_{ls}, by the catalytic current, $(i_s - i_{s0})$, the so-defined β parameter, as a function of the quantum yield $\eta = \eta_r$, and $\eta_r\eta_2/2$ are reported in Figure 12.

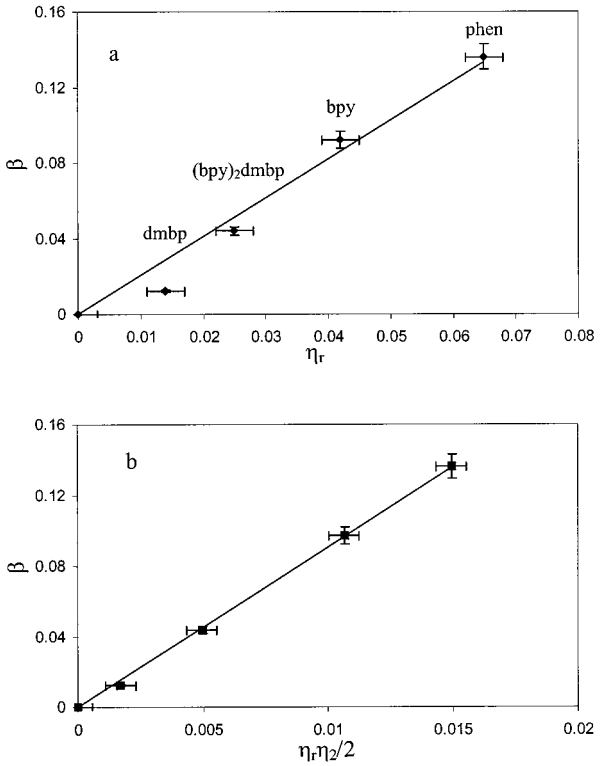

Figure 12. Variation of β with (a) the quantum luminescence efficiency, η_r, and (b) the quantum ECL efficiency $\eta = \eta_r\eta_{2*}/2$. Same conditions as those in Figure 10.

A simple consideration of the quantum luminescence efficiency, η_r, does not produce a good fit for the species showing lower emission (complexes containing the 4,4′-dimethyl-2,2′-bpyridine) (Figure 12a). However, when the overall quantum yield $\eta_r\eta_2/2$ is taken into account, a good correlation is found for all of the species (Figure 12b). The calculated quantum efficiency of the global ECL process, found to be about 25%, is somewhat higher than the reported value of 2%.[2a] This difference could be related to the poor accuracy of the reorganization energy of $CO_2^{\bullet-}$ oxidation and the arbitrariness of the kinetic constants used for its rationalization.[49] However, it is noteworthy that such high reorganization energy is a

determining factor for the explanation of the low ECL efficiency in the Ru(bpy)/oxalate system. The trends observed lend confidence to our analysis of the ECL process and its relation to the observed electrochemical current.

Conclusion

Because the direct oxidation of oxalate can be avoided at oxidized Pt or carbon fiber ultramicroelectrodes, we were able to mediate this oxidation by means of redox catalysis with several coordination compounds. The observed catalytic efficiencies indicated that the homogeneous oxidation was kinetically controlled by the first homogeneous ET. The estimated rate constants were shown to vary with the pH and the ionic strength of the medium. These effects are attributed to the oxalate acid/base properties and ion pair formation in agreement with previous reports of similar studies. When the redox couple was a Ru species, the homogeneous oxidation produced light emission (ECL). The intensity of the steady emitted light correlated with the steady-state current at an ultramicroelectrode, and thus to the catalytic efficiency of the reaction. These relationships show that the emitted light is first governed by the first homogeneous ET between $RuL'L_2^{3+}$ and $C_2O_4^{2-}$ which acts as the rate-determining step for either the current or the light measurements. This finding leads to the conclusion that the pH and ionic strength dependence of the light intensity are approximately due to changes in the first ET rate constant with these parameters. The rate of the first ET reaction investigated in this study, as well as in previous luminescence quenching experiments, were shown to follow Marcus theory. The oxalate dianion is thus oxidized via an outer-sphere ET; the standard potential for the one-electron oxidation was estimated as 1.41 V vs NHE.

The luminescent emission of ECL events can then be related to the driving force of the first ET, but also to the competition between the different pathways of $CO_2^{\bullet-}$ reaction. Because of the high reorganization changes implied in $CO_2^{\bullet-}$ oxidation, ground-state and excited-state formation of the Ru(II) species are the main reactions, with reaction with $Ru(bpy)_3^{2+}$ playing a minor route. The competition between these steps explains the observed ECL efficiencies. The idea that the light intensity in coreactant systems is mainly dictated by the driving force for the first ET should allow the establishment of structure−activity relationships for ECL in these systems. Such relationships should prove useful in the development of more efficient ECL systems and a better understanding and improvement of the existing ones.

Acknowledgment. The support of this work by grants from IGEN, the National Science Foundation, and the Robert A. Welch Foundation is gratefully acknowledged.

References and Notes

(1) (a) Faulkner, L. R.; Bard, A. J. In *Electroanalytical Chemistry*; Bard, A. J., Ed.; Marcel Dekker: New York, 1977; Vol. 10, p 1. (b) Knight, A. W.; Greenway, G. M. *Analyst* **1994**, *119*, 879.

(2) (a) Rubinstein, I.; Bard, A. J. *J. Am. Chem. Soc.* **1981**, *103*, 512. (b) Rubinstein, I.; Bard, A. J. *J. Am. Chem. Soc.* **1981**, *103*, 5007. (c) Rubinstein, I.; Martin, C. R.; Bard, A. J. *Anal. Chem.* **1983**, *55*, 1580.

(3) (a) Marcus, R. A. *J. Chem. Phys.* **1956**, *24*, 966. (b) Marcus, R. A. *J. Chem. Phys.* **1956**, *24*, 979. (c) Marcus, R. A. *J. Chem. Phys.* **1965**, *43*, 679.

(4) (a) Savéant J.-M. *J. Am. Chem. Soc.* **1987**, *109*, 6788. (b) Savéant J.-M. Dissociative Electron Transfer. In *Advances in Electron-Transfer Chemistry*; Mariano, P. S., Ed.; JAI Press: New York, 1994; pp 53−116.

(5) (a) Prasad, D. R.; Hoffman, M. Z.; Mulazzani, Q. G.; Rodgers, M. A. J. *J. Am. Chem. Soc.* **1986**, *108*, 5135. (b) Mulazzani, Q. G.; D'Angelantino, M.; Venturi, M.; Hoffman, M. Z.; Rodgers, M. A. J. *J. Phys. Chem.* **1986**, *90*, 5347.

(6) Steffan, C. R.; Bakac, A.; Espenson, J. H. *Inorg. Chem.* **1989**, *28*, 2992.

(7) Mukhopadhyay, S.; Chaudhuri, S.; Das, R.; Banerjee, R. *Can. J. Chem.* **1993**, *71*, 2155.

(8) Sun, H.; Hoffman, M. Z. *J. Phys. Chem.* **1994**, *98*, 11719.

(9) Pina, F.; Mulazzani, Q. G.; Venturi, M.; Ciano, M.; Balzani, V. *Inorg. Chem.* **1985**, *24*, 848.

(10) Fan, F.-R. F.; Cliffel, D.; Bard, A. J. *Anal. Chem.* **1998**, *70*, 2941.

(11) (a) Braddock, J. N.; Meyer, T. J. *J. Am. Chem. Soc.* **1973**, *95*, 3158. (b) Lin, C.-T.; Bottcher, W.; Chou, M.; Creutz, C.; Sutin, N. *J. Am. Chem. Soc.* **1976**, *98*, 6536. (c) Sprintschnick, G.; Sprintschnick, H. W.; Kirsch, P. P.; Whitten, D. G. *J. Am. Chem. Soc.* **1977**, *99*, 4947.

(12) Bard, A. J.; Fan, F.-R. F.; Mirkin, M. V. In *Electroanalytical Chemistry*; Bard, A. J., Ed.; Marcel Dekker: New York, 1994; Vol. 18, p 243.

(13) Andrieux, C. P.; Savéant, J.-M. In *Electrochemical Reactions in Investigation of Rates and Mechanisms of Reactions, Techniques of Chemistry*; Bernasconi, C. F., Ed.; Wiley: New York, 1990.

(14) Butler, J.; Henglein, A. *Radiat. Phys. Chem.* **1980**, *15*, 603.

(15) (a) Delmastro, J. R.; Smith D. E. *J. Phys. Chem.* **1967**, *71*, 2138. (b) Fleischmann, M.; Lasserre, F.; Robinson, J.; Swan, D. *J. Electroanal. Chem.* **1984**, *177*, 97. (c) Fleischmann, M.; Pletcher, D.; Denuault, G.; Daschbach, J.; Pons, S. *J. Electroanal. Chem.* **1989**, *263*, 225.

(16) Andrieux, C. P.; Dumas-Bouchiat, J. M.; Savéant J.-M. *J. Electroanal. Chem.* **1980**, *113*, 1.

(17) Andrieux, C. P.; Dumas-Bouchiat, J. M.; Savéant, J.-M. *J. Electroanal. Chem.* **1978**, *87*, 39.

(18) When the catalytic efficiency is high, one may roughly assume that the concentration of P is almost constant in the reaction layer and equal to $[P]^0$.16 If so, the diffusion equation becomes similar to eq 6 with $2k_0k_1/k_{-0}[Ox]^0/[P]^0$ instead of $2k_0[Ox]^0$, producing an expression for the catalytic efficiency, showing a dependence on both $[P]^0$ and $[Ox]^0$.

(19) Bard, A. J.; Faulkner, L. R. *Electrochemical Methods*; Wiley: New York, 1980.

(20) *Handbook of Chemistry and Physics*, 72nd ed.; CRC: Cleveland, OH, 1991−92.

(21) (a) Sutin, N.; Creutz, C. *Adv. Chem. Ser.* **1978**, *168*, 1. (b) Sutin, N. *Acc. Chem. Res.* **1982**, *15*, 273. (c) Sutin, N. *Prog. Inorg. Chem.* **1983**, *30*, 441. (d) Krishnan, C. V.; Creutz, C.; Schwarz, H. A.; Sutin, N. *Inorg. Chem.* **1983**, *105*, 5617.

(22) For a review on ET in ion pairs: Billing, R.; Rehorek, D.; Hennig, H. *Top. Current Chem.* **1990**, *158*, 152−199, and references therein.

(23) (a) Fuoss, R. M. *J. Am. Chem. Soc.* **1958**, *80*, 5059. (b) Eigen, M. *Z. Phys. Chem.* **1954**, *1*, 176.

(24) Young, R. C.; Keene, F. R.; Meyer, T. J. *J. Am. Chem. Soc.* **1977**, *99*, 2468.

(25) Endicott, J. F. In *Encyclopedia of Inorganic Chemistry*; King, B. R., Ed.; Wiley: Chichester, 1994; pp 1081−1098.

(26) Pederson, B. F.; Pederson, B. *Acta Chem. Scand.* **1964**, *18*, 1454.

(27) Krishnan, C. V.; Brunschwig, B. S.; Creutz, C.; Sutin, N. *J. Am. Chem. Soc.* **1985**, *107*, 2005.

(28) (a) This approximation is reasonable because SO_4^{2-} and $C_2O_4^{2-}$ have very similar radii,[28b] indicating a similar ion-pairing effect by $H_2PO_4^-$ and HPO_4^{2-}. (b) Pringle, G. E.; Broadbent, T. A. *Acta Crystallogr.* **1965**, *19*, 426.

(29) (a) Noffsinger, J. B.; Danielson, N. D. *Anal. Chem.* **1987**, *59*, 865. (b) Leland, J. K.; Powell, M. J. *J. Electrochem. Soc.* **1990**, *137*, 3127. (c) McCord, P.; Bard, A. J. *J. Electroanal. Chem.* **1991**, *318*, 91.

(30) (a) White, H. S.; Bard, A. J. *J. Am. Chem. Soc.* **1982**, *104*, 6891. (b) Ege, D.; Becker, W. G.; Bard, A. J. *Anal. Chem.* **1984**, *56*, 2413.

(31) Chang, M.; Saji, T.; Bard, A. J. *J. Am. Chem. Soc.* **1977**, *99*, 5399.

(32) Feldberg, S. W. *J. Phys. Chem.* **1966**, *70*, 3928.

(33) Malins, C.; Vandelois, R.; Walton, D.; Donckt, E. V. *J. Phys. Chem. A* **1997**, *101*, 5063.

(34) The production rate of Ru^{3+} at the electrode is related to the current $i_s = nF\upsilon\ \partial[Ru^{3+}]/\partial t$.[19] The production rate of Ru^{3+} that will undergo the catalytic oxidation, $\partial[Ru^{3+}]_{cat}/\partial t$ is then related to $i_s - i_{s0}$ by the same kind of equation, $i_s - i_{s0} = nF\upsilon\ \partial[Ru^{3+}]_{cat}/\partial t$.

(35) Richter, M. M.; Debad, J. D.; Striplin, D. R.; Crosby, G. A.; Bard, A. J. *Anal. Chem.* **1996**, *68*, 4370.

(36) Eberson, L. E. Electron-Transfer Reactions in Organic Chemistry. In *Reactivity and Structure, Concepts in Organic Chemistry;* Hafner, K., Lehn, J.-M., Rees, C. W., von Ragué Schleyer, P., Trost, B. M., Zahradník, R., Eds.; Springer-Verlag Press: Berlin, 1987; Vol. 25.

(37) (a) The difference in BDFE, the bond dissociation free energy, between the oxalic acid and the oxalate dianion, can be estimated using thermodynamic cycles and the corresponding acid dissociation constants of the oxalic acid and of the carbon dioxide radical anion $CO_2^{\bullet-}$ ($pK_{a,CO_2^{\bullet-}} = 1.4$[b]): $BDFE_{C_2O_4H_2} - BDFE_{C_2O_4^{2-}} = RT/F\ \ln 10(pK_{a1} + pK_{a2} - 2 \times pK_{a,CO_2^{\bullet-}}) = 0.15$ eV; assuming similar entropic terms, one could roughly

assimilate this difference with the difference in bond dissociation energy when passing from the oxalic acid to its dianion. (b) Buxton, C. V.; Sellers, R. M. *J. Chem. Soc., Faraday Trans. 1* **1973**, *69*, 555.

(38) Young, R. C.; Keene, F. R.; Meyer, T. J. *J. Am. Chem. Soc.* **1977**, *99*, 2468.

(39) Galus, Z. In *Standard Potentials in Aqueous Solution*; Bard, A. J., Parsons, R., Jordan, J., Eds.; Marcel Dekker: New York, 1985.

(40) (a) Amatore, C.; Savéant, J.-M. *J. Am. Chem. Soc.* **1981**, *103*, 5021. (b) Roberts, J. L.; Sawyer, D. T. *J. Electroanal. Chem.* **1965**, *9*, 1. (c) Russel, P. G.; Novac, N.; Srinivasan, S.; Steinberg, M. *J. Electrochem. Soc.* **1977**, *124*, 1329.

(41) Wallace, W. L.; Bard, A. J. *J. Phys. Chem.* **1979**, *83*, 1350.

(42) Schwarz, H. A.; Creutz, C.; Sutin, N. *Inorg. Chem.* **1985**, *24*, 433.

(43) Nehsvad, G.; Hoffman, M. Z. *J. Phys. Chem.* **1989**, *93*, 2445.

(44) (a) D'Angelantonio, M.; Mulazzani, Q. G.; Venturi, M.; Ciano, M.; Hoffman, M. Z. *J. Phys. Chem.* **1991**, *95*, 5121. (b) Venturi, M.; Mulazzani, Q. G.; D'Angelantonio, M.; Ciano, M.; Hoffman, M. Z. *Radiat. Phys. Chem.* **1991**, *37*, 449.

(45) Frank, A.; Gratzel, M.; Henglein, A.; Janata, E. *Ber. Bunsen-Ges. Phys. Chem.* **1976**, *80*, 294.

(46) Creutz, C.; Sutin, N. *J. Am. Chem. Soc.* **1977**, *99*, 241.

(47) The yield of the ECL process is $\eta_r\eta_2/2$ because two electrons transfer per molecule of $C_2O_4^{2-}$ to generate light, the first one leading to the formation of $CO_2^{\bullet-}$, with the second one strictly related to the competition between k_2 and k_2*.

(48) (a) For a review of these data, Juris, A.; Balzani, V.; Barigelletti, F.; Campagna, S.; Belser, P.; Von Zelewsky, A. *Coord. Chem. Rev.* **1988**, *84*, 85. (b) McClanahan, S. F.; Dallinger, R. F.; Holler, F. J.; Kincaid, J. R. *J. Am. Chem. Soc.* **1985**, *107*, 4853. (c) Nakamaru, K. *Bull. Chem. Soc. Jpn.* **1982**, *55*, 2697.

(49) A 0.2 eV (5%) decrease in the reorganization energy leads to a 14% ECL efficiency.